MANSOURA JOURNAL OF CHEMISTRY
Official Journal of Faculty of Science, Mansoura University, Egypt
E-mail: scimag@mans.edu.eg ISSN: 1687-5060

Facile Synthesis of Cu vanadate/ZnO Nanoparticles by Sol-Gel Method for Photocatalytic Degradation of Methylene Blue Dye

M. Sayed[1], M.A. Ahmed[2] & E. Elsherbeny[2]*

[1.] *Heliopolis Company for Chemical Industries, Cairo, Egypt*
[2.] *Chemistry Department, Faculty of Science, Ain Shams University, Cairo, Egypt*
*** Correspondence to:** *M. Sayed; mostafasayed7141@yahoo.com, Tel.: 01155546081*

Received:4/1/2023
Accepted: 22/1/2023

Abstract: Here, utilizing copper vanadate/zinc oxide (CuVA/ZnO) nanoparticles, we looked into the photocatalytic degradation of the dye methylene blue from an aqueous solution. For remarkable photocatalytic degradation of the dye methylene blue (MB), pure zinc oxide and copper vanadate doped zinc oxide nanopowders (5 wt.% Cu vanadate) were created. Sol-gel was used to create a single phase of zinc oxide (ZnO). Meanwhile, using a sonochemical process, the new copper vanadate nanoparticles were easily created and integrated onto the surface of ZnO. X-ray diffraction (XRD), N_2 adsorption-desorption isotherm, photo luminescence (PL), and high-resolution transmission electron microscopy (HRTEM) were used to evaluate and characterize the prepared CuVA/ZnO. Successful dispersion of the copper vanadate phase between ZnO nanocrystals was confirmed by XRD. The TEM pictures further demonstrated the hexagonal wurtzite structure of the as-produced CuVA/ZnO nanoparticles and highlighted the homogeneous integration of copper nanoparticles on the surface of ZnO. Along with an increase in ZnO's surface area, other textural metrics also improved as a result. All of the results obtained underscored the copper vanadate nanoparticles' synergistic impact on the physicochemical characteristics of ZnO. Under UV, solar, and visible light irradiations, CuVA/ZnO shown better performance against MB photodegradation**.**

keywords: Zinc oxide nanoparticles; Sol-gel; Copper vanadate; photocatalytic removal; Methylene blue; Water treatment

1. Introduction

The world needs clean water for irrigation and consumption. Recent attention has been focused on the health risks posed to people and other living things by organic dye discharges from the textile dyeing, paper producing, paints, cosmetics, and food processing sectors. [1-3] The release of effluents containing poorly biodegradable dyes into water bodies is undesirable due to their hazardous byproducts created during hydrolysis and oxidation processes in the wastewater phase. [4-6] The aquatic flora and wildlife are impacted by dyes entrance into the water supplies, disrupting the ecology. Since these dyes are resistant to biodegradation and persist in water for a long time, it is necessary to convert them into simple molecules. This was made possible by the photoinduced breakdown of these dyes, which was facilitated by a number of photocatalysts. [7,8]

Coagulation, adsorption, flocculation, advanced oxidation, and precipitation are some of the classic methods for treating wastewater that not only take a long time to complete but also produce secondary sludge that is expensive to dispose of. [9,10] Photocatalytic degradation of organic pollutants has attracted a lot of interest among the different techniques for treating dye-contaminated water. [11,12] In recent years, nanomaterials in their different forms, shapes, and sizes have been discovered to be efficient in the removal of dye contaminants through photocatalytic activities. [13,14] This is attributed to their unique physicochemical properties such as their structures, high mechanical strength, high width-to-height ratio, high thermal and

electrical conductivities, slight advantage metal/semi-metallic weight and behavior, and high surface area [15-19].

Metal oxide nanocomposites, in particular, have been widely utilized in environmental research due to their huge applications, including catalysis and sensing applications [20,21]. ZnO is a popular material among many research teams as they act as a versatile platform and play a pivotal role in several sectors of nanotechnology [22,23]. ZnO is the preferred metal oxide as it offers a wide direct bandgap (~3.37 eV), a superior piezoelectric coefficient as well as a high UV-sensitive n-type semiconductor [24]. Zinc oxide and its nanostructures with advanced nanotechnology approaches have paved the way for several important applications ranging from laser diodes, photocatalysts, photovoltaics, and piezoelectric energy harvesters [25-28]. In the field of water treatment, ZnO nanoparticles have proved itself as a promising photocatalyst that can decompose the toxic dyes through a photocatalytic reaction under the UV irradiation. Nonetheless, ZnO has several drawbacks in terms of the fast electron-hole pair recombination and the wide band gap [29-31]. These shortcomings limit its industrial applications. Therefore, several reports have been released annually and focused to the electron-hole pair recombination phenomena via doping with other transition metals ex. Aluminium [32], cobalt [33], nickel [34], and copper [35,36].

Copper vanadates are a class of catalysts with band gap of ~2 eV, making them suitable for visible light absorption [37]. They thus exhibit dye degradation activity as photocatalysts [38-39] and water splitting property as photoanode candidates [40-42]. Accordingly, the main goal of this study is to improve the photocatalytic efficiency of ZnO via doping with hetero atoms. In this work, CuV_2O_6 nanoparticles, was selected as a dopant for zinc oxide. This hybrid (CuVA/ZnO nanoparticles) was prepared using sol–gel method. The physiochemical characteristics of the fabricated nanoparticle were characterized by XRD, TEM and surface area. Finally, the synthesized nanoparticle was employed in the photocatalytic degradation of methylene blue (MB) dye.

2. Materials and methods

2.1. Materials

Zinc acetate [Zn $(CH_3COO)_2.5H_2O$], Tween-80 [$C_{32}H_{60}O_{10}$], ammonia solution (25%), copper chloride [$CuCl_2$], ammonium vanadate [NH_4VO_3] were purchased from Sigma-Aldrich company. Methylene blue ($C_{16}H_{18}ClN_3S$), MW 319.85 g/mol, 95 % pure was purchased from Jiangxi, China. The structure of methylene blue is shown in Fig.1.

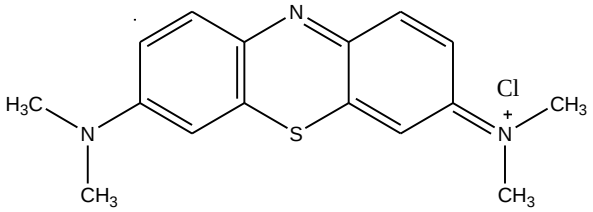

Fig.1. Structure of Methylene blue

2.2. Material Characterization

The specific surface area (BET) of the prepared samples was determined according to Brunauer–Emmett–Teller equation via adsorption of N_2 by the sample on a Quantochrome Nova-Touch 4LX automated gas-sorption apparatus (USA) at 77K. Meanwhile, the pore size was calculated from the desorption isotherm according to the Barrett, Joyner, and Halenda (BJH) mode. Also, the high-resolution transmission electron microscope (HRTEM, JEOL Ltd., 6340, Tokyo-Japan) was used to investigate the obtained morphology. The spectrum of diffuse reflectance spectroscopy (DRS) for the obtain hybrid compared with pristine was detected on JASCO spectrometer (V-570). Moreover, photoluminescence bands were acquired on Lumina Fluorescence spectrometer, (Thermo Fisher Scientific - UK). The optical characteristics of the prepared nanoparticles as well as the removal percentage of MB were evaluated with JASCO spectrometer (V-570).

2.3. Preparation of zinc oxide nanoparticles

Zinc oxide nanoparticles (ZnO NPs) were prepared by sol-gel method using Tween-80 as an emulsifier. In the typical method, 50 g of zinc acetate were dissolved in 150 ml distilled water under vigorous stirring. After 60 min., 20 ml of Tween-80 (10 v/v %) was inserted and left stirred for further 60 min. for homogeneous mixing. Then, few drops of freshly prepared ammonia solution, 3M, were

carefully added and kept under a continuous stirring for three hrs, till a colloidal suspension is obtained, followed by aging for 48 hrs. After that, the mixture was filtered out and well washed with distilled water. Finally, the solid particles were collected and dried in the oven at 100°C overnight. For crystallization, the dried sample was transferred to the muffle furnace and calcinated at 400°C for 2 hrs.

2.4. Preparation of copper vanadate nanoparticles (CuV_2O_6)

Briefly, copper vanadate nanoparticles (CuV_2O_6 NPs) were prepared by mixing of equimolar concentrations of copper chloride ($CuCl_2$) and ammonium vanadate in distilled water under vigorous stirring for 3 hrs. Then, the mixture was homogenised with the ultrasonic bath for 2 hrs in order to well distribute the obtained particles. Finally, the colloidal suspension of CuV_2O_6 nanoparticles was filtered out, well washed with the distilled water, and dried in the oven at 100°C overnight.

2.5. Preparation of CuV_2O_6/ ZnO nanoparticles (CuVA/ZnO)

The hybrid particles based CuV_2O_6 and ZnO (CuVA/ZnO) were obtained by solution mixing. In this preparation, various proportions of the as-synthesized copper vanadate nanoparticles were added to the prepared zinc oxide nanoparticles of a certain weight in distilled water under vigorous stirring for 30 min. Finally, the sample was filtered out, well washed, and dried in the oven at 100°C overnight. The samples codes ZnO and CuVA/ZnO are denoted to the pure ZnO and the hybrid particles containing 5 wt. % of CuV_2O_6, respectively.

2.6. Photocatalytic activity test

The photocatalytic degradation of methylene blue (MB) dye was performed under UV and sunlight irradiations. The ultra-violet emission was obtained from high-pressure mercury lamp of intensity 8-Watt and wavelength 365 nm. The initial dye concentration used was 2×10^{-5} mol/L. However, at the first and in order to achieve the adsorption/desorption equilibrium, the dye solution was shacked for 1 hr. in presence of 0.1 g of CuVA/ZnO. Subsequently, the mixture was irradiated under either UV or sunlight and the conditions were optimized. Moreover, the photocatalytic reaction was done under visible light using a xenon lamp of intensity 100 W and a cut-off filter to remove UV radiation ($\lambda \leq 420$ nm). The remained dye was generally measured by UV-vis spectrophotometer by following the gradual decline of the MB maximum absorption peak intensity appears at 664 nm over the reaction time. Particularly, in case of using sunlight irradiation, the sample was put in 200 mL quartz reactor that placed on our laboratory platforms and the photocatalytic process was started at 2 a.m. for 3 hrs at temperature ranged between 30 and 35°C. On the other hand, the concentration of the produced hydroxyl radicals was measured using photoluminescence in the presence of terephthalic acid (TPA) that could react with the radical species forming 2-hydroxyterephthalic acid (2-HTA) detected at a fixed wavelength.

3. RESULTS AND DISCUSSION

3.1. X-rays Diffraction

XRD is a reliable and widespread technique which is extensively involved in the investigation of the crystalline parameters and size of the nanoparticles. Figure 2 displays XRD of the as-synthesized samples. ZnO spectrum displays characteristics bands at 2θ = 31.5° (100), 34.3° (002), 36.4° (101), 47.8° (102), 56° (110), 62.8° (103), 66.2° (200), 67.8° (112), and 69.3° (201), Fig.2[A], confirming the successful formation of ZnO nanoparticles with Wurtzite cubic structure (JCPDS no. 36-1451). Fig.2[B] shows characteristic XRD pattern of triclinic CuV_2O_6 with a space group C-1 (PDF Card No: 01–074–2117) [43].

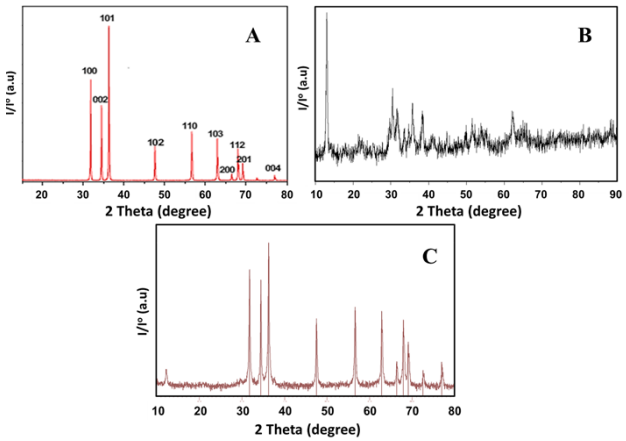

Fig.2: XRD pattern of [A] ZnO, [B] CuV_2O_6, and [C] CuVA/ZnO nanocomposites.

The major XRD patterns are centered at angle (2θ) 29° (201), 32° (1–11), 34° (111), 42° (−203), 52° (020), 58° (2–11), and 63° (−5–13), approximately. Additionally, CuV_2O_6 nanoparticles were obtained with a lower crystallinity and showed a distinctive pattern at 2θ = 14° as shown in Fig.2[B]. Particularly, this peak was found in Fig.2[C] of CuVA/ZnO. These results emphasized the well dispersion of CuV_2O_6 nanoparticles between zinc oxide crystallites.

3.2. High Resolution Transmission electron microscope (HRTEM)

Morphological properties, including size and shape, have critical roles in the physicochemical activities of nano particles. Therefore, the prepared ZnO and CuVA/ZnO nanocomposites were investigated via TEM analysis to determine their respective sizes and shapes as illustrated in Fig.3. The micrographs reveal the formation of mixture shape ZnO nanoparticles, rods (red arrows) and quasi spherical (blue arrows), with a size ranging between 36 and 92 nm; Fig.3[A]. The electron diffraction micrograph showed high polycrystallinity of the obtained ZnO NPs, Fig.3[C]. Obviously, the morphology was quite changed upon loading of CuV_2O_6 on the ZnO crystal. As shown in Fig.3[B],

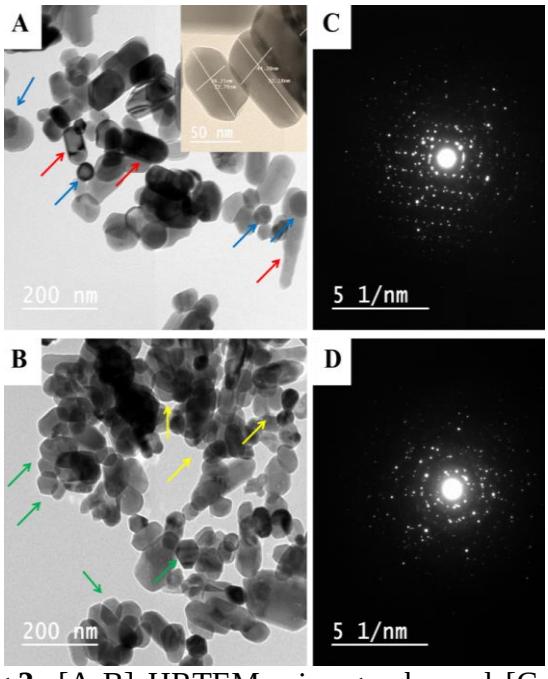

Fig.3: [A-B] HRTEM micrographs and [C-D] Electron diffraction of ZnO and CuVA/ZnO, respectively. Inset image is higher magnification.

Wurtzite nanoparticles of hexagonal shape (green arrows) were observed in addition to some spherical particles (yellow arrows). Indeed, these results indicate that a strong interaction between ZnO and CuV_2O_6 nanoparticles with a homogeneous dispersion was established. Moreover, the electron diffraction taken for these crystals emphasized a lower crystallinity compared to pure ZnO NPs in agreement with XRD findings.

3.3. Surface Area

The obtained ZnO NPs and their doped form had their specific surface areas assessed (CuVA/ZnO). The results show that the surface area has increased following doping with CuV_2O_6, as indicated by the measurements of 7.7 and 9.2 m^2/g for ZnO and CuVA/ZnO, respectively. Additionally, for ZnO and CuVA/ZnO, the total pore volume changed from 1.2644 x 10^{-2} to 1.5073 x 10^{-2} cc/g, respectively. As is common knowledge, increasing the nanoparticles' surface area causes the generation of reactive oxygen radicals needed for dye degradation [44].

3.4. Optical Properties

Diffuse reflectance spectroscopy spectra (DRS) for CuVA/ZnO nanoparticles are illustrated in Fig.4 [A]. As shown, strong absorption bands for ZnO NPs and its corresponding hybrid containing 5 wt.% of copper were observed in the region ranged from 200 to 400 nm as a result of electron transfer from the valence band to the conduction band. Particularly, ZnO NPs displayed a sharp absorption at ~400 nm due to its intrinsic UV absorption. However, introduction of copper nanoparticles showed a slight shift to the visible region confirming the successful formation of the hybrid. The same observation was detected from the photoluminescence spectra, Fig.4 [B], as a slight decreasing in the intensity of ZnO NPs after incorporation of copper vanadate nanoparticles. This might be revealed to the reduction in the electron-hole recombination rate and hence increasing the lifetime of the generated reactive species. Indeed, the low shift in the main peak observed either in the DRS or in the photoluminescence was not clearly significant i.e. this might due to the low copper content.

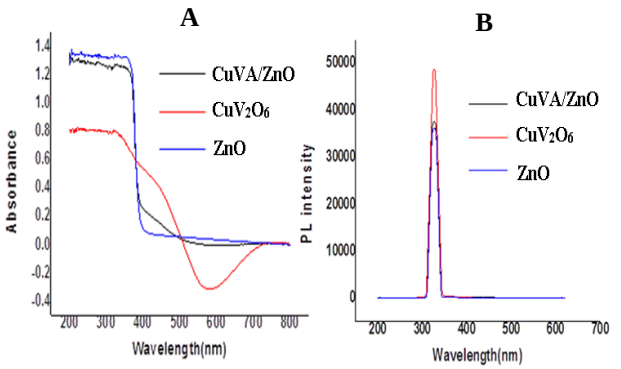

Fig.4: [A] Diffuse reflectance spectra and [B] Photoluminerence spectra for ZnO, CuV_2O_6, and CuVA/ZnO.

3.5. UV-Photocatalytic degradation of MB over ZnO and CuVA/ZnO

Under UV irradiation, the photocatalytic activity of ZnO, CuV_2O_6, and their hybrid CuVA/ZnO was assessed. Fig.5 displays the following: (I) In the dark, ZnO responds sporadically. The degradation began as soon as it was exposed to UV light and progressed to up to 70%. (II) The breakdown of MB was reported at 93% after two hours of treatment with CuVA/ZnO, indicating that the addition of copper NPs increased the photocatalytic activity of ZnO. The primary drawback of ZnO is, in fact, its rapid electron-hole recombination rate, which is thought to be the cause of its reduced photoactivity.

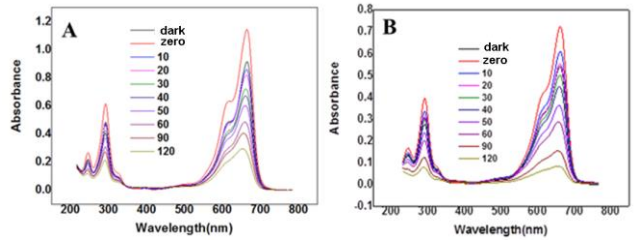

Fig.5: Removal of MB after the photocatalytic degradation under UV irradiation over [A] ZnO, and [B] CuVA/ZnO nanocomposite.

While CuV_2O_6 NPs were inserted, the electron-hole recombination could be suppressed. Particularly, ZnO can absorb the UV energy and the electrons are transferred from the valance band leaving holes to the conduction band. The photo-excited electrons were then trapped by copper vanadate NPs to its Fermi level i.e. control the electron-hole recombination. Then, the reactive oxygen species (ROS) can be generated via reduction of dissolved oxygen at the conduction band and combination of water molecules with the holes at the valance band. These radicals could degrade the dye molecules through hydrogen abstraction and subsequent oxidation processes. On more reason behind this superior behaviour is the increment in the surface area and the total pore size after the introduction of copper NPs which allow adsorbing more dye molecules to be degraded on the surface of the prepared CuVA/ZnO as shown in Fig.6.

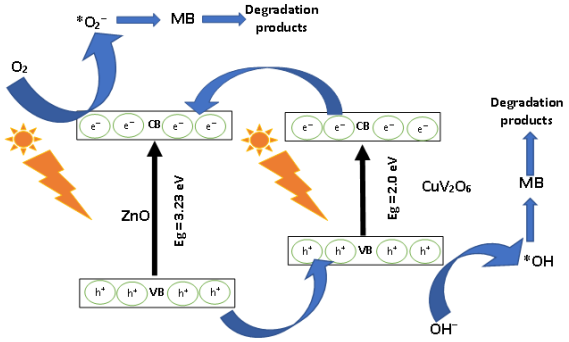

Fig.6: The possible degradation mechanism of CuVA/ZnO photocatalyst

3.6. Solar-Photocatalytic degradation of MB over ZnO and CuVA/ZnO

When exposed to sun light, the produced hybrid was tested for resistance to MB breakdown in comparison to pure ZnO NPs. The following can be seen in Fig.7: (I) ZnO nanoparticles don't degrade MB in any way. (II) When copper nanoparticles were added, ZnO nanoparticles' photocatalytic activity increased when MB was broken down under sun radiation. These results did in fact support CuV_2O_6 NPs' synergistic action. The insertion of copper vanadate nanoparticles changed the absorption response to visible light, which may be the cause of this behaviour. CuVA/photocatalytic ZnO's mechanism under sun irradiation can be anticipated to be deep. In a short, the hybrid contains semiconductor nanoparticles with conduction and valance bands made of copper and zinc. The solar energy needed for excitation from the valance to the conduction band is absorbed by the electrons in the NPs. Then, because it has been noted that copper has a lower band gap and band locations than zinc, the photogenerated electrons were moved from the conduction band of copper NPs to the conduction band of ZnO. In the meantime, the zinc NP holes that emerge from this move to the copper particle valance band. This indicates that the conduction

band is occupied by electrons and the valance band by holes. This makes it easier to reduce the dissolved oxygen at the conduction band and oxidise water molecules at the valance band, resulting in superoxide $*O_2^-$ and *OH, which are oxygen and hydroxyl radicals, respectively. Due to their high reactivity, these radicals could damage dye molecules and speed up the degradation process. Finally, it could be asserted that the created hybrids may exhibit various electron pathways when exposed to UV and solar rays, as opposed to UV's method of breakdown.

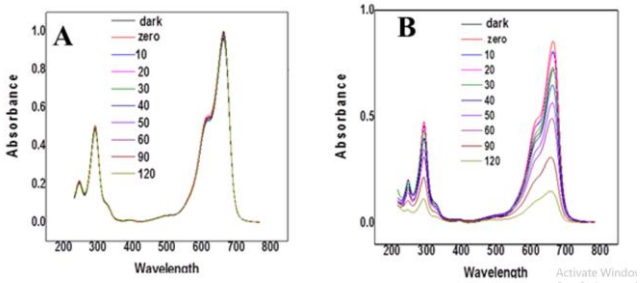

Fig.7: Removal of MB after the photocatalytic degradation under solar irradiation over [A] ZnO and [B] CuVA/ZnO nanocomposite.

3.7. Photocatalytic degradation of MB under visible light

The incorporation of copper vanadate NPs into ZnO NPs led to a slight shift to a visible region. Thus, the photocatalytic reactivity of CuVA/ZnO was assessed under visible light irradiation using xenon lamp. As shown in Fig.8, the results confirmed the degradation of MB up to ~ 70 % over the two hours of irradiation upon the incorporation of only 5 wt.%CuV_2O_6 on the ZnO surface. This ensures the effect of CuV_2O_6 on the ZnO photocatalytic reactivity.

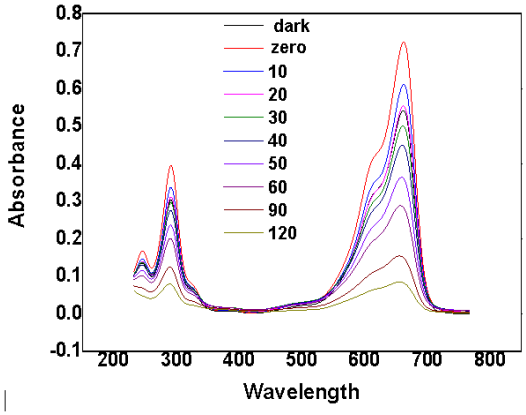

Fig.8: Removal of MB after the photocatalytic degradation under visible light irradiation over CuVA/ZnO.

3.8. OH radical detection

Given their high reactivity and instability, hydroxyl radicals (OH) play a significant part in the breakdown of organic dyes. The detection of hydroxyl radicals was carried out using terephthalic acid as a probe molecule. OH radicals are created during the photodegradation reaction, and this can be seen using a quick and easy photoluminescence approach. Terephthalic acid was added as a probe molecule that could interact with the hydroxyl radicals present in the reaction mixture to form 2-hydroxyterephthalic acid, allowing the amount of hydroxyl radicals produced during the degradation reaction to be measured. The amount of 2-hydroxyterephthalic acid generated was calculated at 425 nm using UV measurement, as shown in Fig.9. It is important to note that 2-hydroxyterephthalic acid, a derivative of terephthalic acid, can produce fluorescence when exposed to light, despite the fact that terephthalic acid is known as a non-fluorescent molecule and lacks an absorption band, particularly after 300 nm. Therefore, it is evident from Fig. 9 that there is no peak for terephthalic acid. However, the 2-hydroxy-terephthalic acid band's intensity rises over time, indicating that the degradation reaction is producing more hydroxyl radicals.

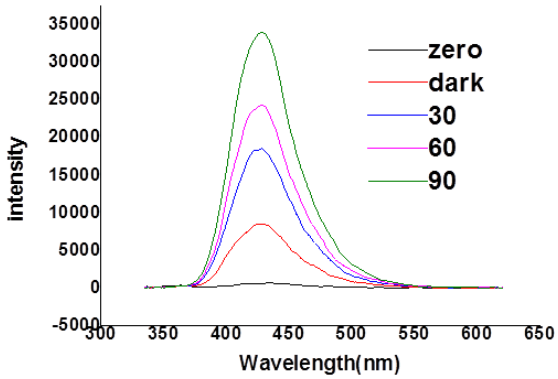

Fig.9: PL spectrum for terephthalic acid on CuVA/ZnO

3.9. The recycle of the photocatalyst

In order to verify the stability of the produced CuVA/ZnO nanoparticles, a series of succeeding photocatalytic cycles were run under ideal circumstances. After every cycle, the photocatalyst was thoroughly cleaned with distilled water to get rid of the dye that had physisorbed onto it. It was then dried at 80°C and utilized in another cycle. According to

Fig.10, the photocatalytic activity remained nearly constant for five cycles.

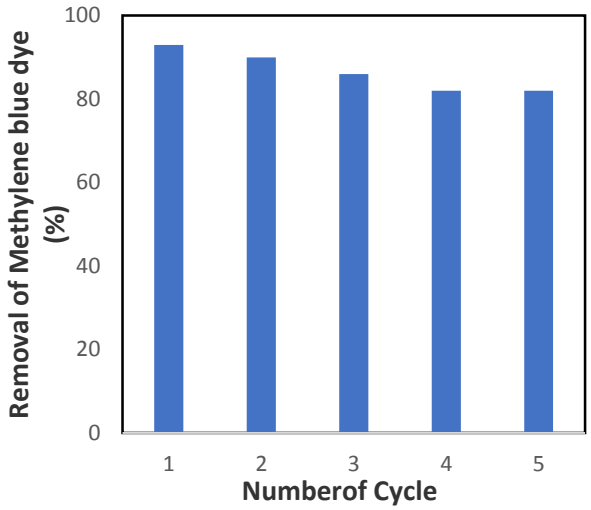

Fig.10 : Recycle of CuVA/ZnO on removal of methylene blue dye.

4. Conclusions

Successful preparation of copper vanadate nanoparticles at 5% by weight in zno nanoparticles. The existence and uniform dispersion of copper vanadate nanoparticles between zno crystals were confirmed by xrd and tem. The shift towards the visible range and the decrease in the rate of electron-hole recombination, respectively, were demonstrated by the drs and photoluminescence experiments. The produced hybrids shown enhanced photocatalytic activity against the degradation of mb during exposure to uv, solar, and visible irradiations. In particular, the hybrid achieved 93% when exposed to uv light. However, under solar light, it got as high as 90%. The increase in surface area and suppression of electron-hole recombination brought about by the synergistic interaction between copper vanadate and zno nanoparticles were recognized with the improvement in the photocatalytic performance. Finally, terephthalic acid was used as a probe molecule to determine the concentration of hydroxyl radicals created during the reaction.

Conflicts of interest

The authors have declared that there is no a conflict of interest.

Acknowledgments

The authors are grateful for ain shams university for the workplace and the facilities required for doing the research.

5. References

1. Miao, Y., Xu, X., Liu, K., Yu, S., Wang, Y., Yang, S. (2020) Preparation and activity evaluation of the novel Cu/TiO_2 nanometer photocatalytic materials. Sci. Adv. Mater. **12**, 1027–1033.
2. Shang, J.; Zou, W., Wang, P., Li, A., Zhou, M., Luo, P., (2021) Preparation and characterization of hollow zinc oxide nanofibers and investigation of its photocatalytic properties. *J. Nanoelectron. Optoelectron.* **16**, 64–71.
3. Wang, B., Zhang, R., Xu, J., Qin, S., Zheng, J., Bian, Y., Liu, Y., Shen, B. (2020). Effect of calcination temperature on light absorption and visible light photocatalytic activity of N doped TiO_2 nano-crystalline. Sci. Adv. Mater. **12**, 449–453.
4. Panimalar, S., Uthrakumar, R., Tamil Selvi, E., Gomathy, P., Inmozhi, C., Kaviyarasu, K., Kennedy, J. (2020) Studies of MnO_2/g-C_3N_4 hetrostructure efficient of visible light photocatalyst for pollutants degradation by sol–gel technique. Surf. Interfaces **20**, 100512.
5. Fuku, X., Matinise, N., Masikini, M., Kasinathan, K., Maaza, M., (2018) An electrochemically active green synthesized polycrystalline NiO/MgO catalyst: Use in photo-catalytic applications. Mater. Res. Bull. **97**, 457–465.
6. Sharma, S.; K. Kumar, N. Thakur, S. Chauhan, M. Chauhan (2020) The effect of shape and size of ZnO nanoparticles on their antimicrobial and photocatalytic activities: a green approach, Bull. Mater. Sci. **43**, 20, 1-10.
7. Shah, A.A.; M.A. Bhatti, A. Tahira, A.D. Chandio, I.A. Channa, A.G. Sahito, E. Chalangar, M. Willander, O. Nur, Z.H. Ibupoto (2020) Facile synthesis of copper doped ZnO nanorods for the efficient photo degradation of methylene blue and methyl orange, Ceram. Int. **46(8)** 9997–10005.
8. Areeb, A.; T. Yousaf, M. Murtaza, M. Zahra, M.I. Zafar, A. Waseem (2021) Green photocatalyst Cu/NiO doped zirconia for the removal of environmental pollutants, Mater. Today Commun. **28**, 102678.

9. Wei, Y.X., Ma, M.G., Li, S.Y., Liu, F., Zhao, G.H. (2020) Visible light activity in phenol degradation of C60@P25 photocatalyst with Core–Shell structure. *J. Nanoelectron. Optoelectron.* **15**, 189–196.
10. MuhudJulkabli, N., Bagheri, S., Bee Abd Hamid, S. (2014). Recent advances in heterogeneous photocatalytic decolourization of synthetic dyes. *Sci. World J.*, 1-25.
11. Saini, M.; Dehiya, B.S.; Umar, A. (2020) VO_2(M)@CeO_2 core-shell nanospheres for thermochromic smart windows and photocatalytic applications. Ceram. Int. **46 (1)**, 986–995.
12. Ma, X., Dang, R., Liu, J., Yang, F., Li, H., Zhang, Y., Luo, J. (2020) Facile synthesis and characterization of spinel $NiFe_2O_4$ nanoparticles and studies of their photocatalytic activity for oxidation of alcohols. Sci. Adv. Mater. **12**, 357–365.
13. Sharma, Shelja, Ibhadon, Alex O., GraziaFrancesconi, M., Kumar Mehta, Surinder, Elumalai, Sasikumar, Kumar Kansal, Sushil, Umar, Ahmad, Baskoutas, S. (2020) Bi_2WO_6/C-dots/TiO_2: A novel Z-scheme photocatalyst for the degradation of fluoroquinolone levofloxacin from aqueous medium. *Nanomaterials*, **20**(910) 1-20.
14. Singh, J.; T. Dutta, K.-H. Kim, M. Rawat, P. Samddar, P. Kumar (2018)'Green' synthesis of metals and their oxide nanoparticles: applications for environmental remediation, *J. Nanobiotechnol.* 16, 84.
15. Salem, S.S.; A. Fouda (2020) Green synthesis of metallic nanoparticles and their prospective biotechnological applications: an overview, *Biol.* Trace Elem. Res. **199**, :344–370
16. Pugazhendhi, A.; R. Prabhu, K. Muruganantham, R. Shanmuganathan, S. Natarajan (2019) Anticancer, antimicrobial and photocatalytic activities of green synthesized magnesium oxide nanoparticles (MgONPs) using aqueous extract of Sargassum wightii, *J. Photochem. Photobiol. B Biol.* **190**:86–97.
17. Shaheen, T.I.; Salem, S.S.; Zaghloul, S. (2019) A new facile strategy for multifunctional textiles development through in situ deposition of SiO_2/TiO_2 nanosols hybrid, Ind. Eng. Chem. Res. 58, 20203–20212.
18. Sharaf, O.M.; Al-Gamal, M.S.; G.A. Ibrahim, N.M. Dabiza, S.S. Salem, M.F. El-ssayad, et al., (2019) Evaluation and characterization of some protective culture metabolites in free and nano-chitosan-loaded forms against common contaminants of Egyptian cheese, Carbohydr. Polym., **223** 115094.
19. Fouda, A.; Hassan, S.E.-D.; Abdo, A.M.; El-Gamal, M.S. (2020) Antimicrobial, antioxidant and larvicidal activities of spherical silver nanoparticles synthesized by endophytic Streptomyces spp, Biol. Trace Elem. Res. **195**:707–724.
20. Lum, P.; Foo, K.; Zakaria, N.; Palaniandy, P. (2020) Ash based nanocomposites for photocatalytic degradation of textile dye pollutants: a review, Mater. Chem. Phys., **241**:122405.
21. Mohamed, A.A.; A. Fouda, M.A. Abdel-Rahman, S.E.-D. Hassan, M.S. El-Gamal, S.S. Salem, et al., (2019) Fungal strain impacts the shape, bioactivity and multifunctional properties of green synthesized zinc oxide nanoparticles, Biocatal. Agric. Biotechnol. **19:**101103.
22. Noman, M.T.; Amor, N.; Petru, M. (2021) Synthesis and applications of ZnO nanostructures (ZONSs): a review. Crit Rev Solid State Mater Sci, **47**:1-43.
23. Verma, R.; Pathak, S.; Srivastava, A.K.; Prawer S, Tomljenovic-Hanic S. (2021) ZnO nanomaterials: green synthesis, toxicity evaluation and new insights in biomedical applications. *J Alloys Compd*, **876**:160175.
24. Wang, Z.L. (2009) ZnO nanowire and nanobelt platform for nanotechnology. Mater Sci Eng R Rep, **64**:33-71.
25. Keis, K.; Bauer, C.; Boschloo, G.; Hagfeldt, A.; Westermark, K.; Rensmo H, et al. (2002) Nanostructured ZnO electrodes for dyesensitized solar cell applications. *J Photochem Photobio A Chem*, **148**:57-64.
26. Ye, C.; Bando Y, Shen G, Golberg D. (2006) Thickness-dependent photocatalytic

performance of ZnO nanoplatelets. *J Phys Chem B*, **110**:15146-51.

27. Zhao, Y.; Deng P, Nie Y, Wang P, Zhang Y, Xing L, et al. (2014) Biomolecule-adsorption-dependent piezoelectric output of ZnO nanowire nanogenerator and its application as selfpowered active biosensor. Biosens Bioelectron, **57**:269-75.
28. Pandey, R.; Maria Joseph Raj NP, Singh V, Iyamperumal Anand P, Kim S-J. (2019) Novel interfacial bulk heterojunction technique for enhanced response in ZnO nanogenerator. ACS Appl Mater Interfaces, **11**:6078-88.
29. Sohrabnezhad, S. and Seifi, A. (2016) The green synthesis of Ag/ZnO in montmorillonite with enhanced photo-catalytic activity, Appl. Surf. Sci. **386**, 33.
30. Rehman, S.; R. Ullah, A.M. Butt, N.D. Gohar, (2009) Strategies of making TiO_2 and ZnO visible light active, *J. Hazard. Mater*. **170(2)** 560.
31. Ahmed, M.A.; M.F. Abdel Messih, E.F. El-Sherbeny, Suzan F. El-Hafez, Aliaa M.M. Khalifa (2017) Synthesis of metallic silver nanoparticles decorated mesoporous SnO_2 for removal of methylene blue dye by coupling adsorption and photocatalytic processes, *J. Photochem. Photobiol.. A.* **346**, 77-88.
32. Mamat, M.H.; M.Z. Sahdan, Z. Khusaimi, A. Zain Ahmed, S. Abdullah, M. Rusop. **(2010)** Influence of doping concentrations on the aluminum doped zinc oxide thin films properties for ultraviolet photoconductive sensor applications. Optical Materials, **32** : 696-699.
33. Ansari, S.A.; Ambreen Nisar, Bushara Fatma, Wasi Khan A.H. Naqvi. (2012) Investigation on structural, optical and dielectric properties of Co doped ZnO nanoparticle synthesized by gelcombustion route. Materials Science and Engineering, **177**: 428-435.
34. El-Hilo, M.; A.A. Dakhel, A.Y. Ali-Mohamed (2009) Room temperature ferromagnetism in nanocrystalline Ni-doped ZnO synthesized by co-precipitation. *Journal of Magnetism and Magnetic Materials*, **321**: 2279 2283.
35. Singhal, S.; Kaur, J.; Namgyal, T.; Sharma, R. (2012) Cu-doped ZnO nanoparticles: Synthesis, structural and electrical properties. Physica B., **407**: 1223-1226.
36. Liu, H.; Jinghai Yang, Zhong Hua, Yongjun Zhang, Lili Yang, Li Xiao, Zhi Xie. (2010) The structure and magnetic properties of Cu-doped ZnO prepared by sol gel method. Applied Surface Science, **256**: 4162-4165.
37. Keerthana, S.P.; Yuvakkumar, R.; Kumar, P.S.; Ravi, G.; Velauthapillai, D. (2022) Surfactant induced copper vanadate (-$Cu_2V_2O_7$, $Cu_3V_2O_8$) for different textile dyes degradation. Environ. Res., **211**, 112964.
38. Khan, I.; Qurashi, A. (2017) Shape Controlled Synthesis of Copper Vanadate Platelet Nanostructures, Their Optical Band Edges, and Solar-Driven Water Splitting Properties. Sci. Rep., **7**, 14370.
39. Wiktor, J.; Reshetnyak, I.; Strach, M.; Scarongella, M.; Buonsanti, R.; Pasquarello, A. (2018) Sizable Excitonic Effects Undermining the Photocatalytic Efficiency of_-Cu2V2O7. *J. Phys. Chem. Lett.*, **9**, 5698–5703.
40. Yan, Q.; Yu, J.; Suram, S.K.; Zhou, L.; Shinde, A.; Newhouse, P.F.; Chen, W.; Li, G.; Persson, K.A.; Gregoire, J.M. (2017) Solar Fuels Photoanode Materials Discovery by Integrating High-Throughput Theory and Experiment. Proc. Natl. Acad. Sci. USA, **114**, 3040–3043.
41. Ghiyasiyan-Arani, M.; Masjedi-Arani, M.; Salavati-Niasari, M. (2016) Facile synthesis, characterization and optical properties of copper vanadate nanostructures for enhanced photocatalytic activity. *J. Mater. Sci. Mater. Electron.*, **27**, 4871–4878.
42. Zhou, L.; Shinde, A.; Newhouse, P.F.; Guevarra, D.; Wang, Y.; Lai, Y.; Kan, K.; Suram, S.K.; Haber, J.A.; Gregoire, J.M. (2020) Quaternary Oxide Photoanode Discovery Improves the Spectral Response and Photovoltage of Copper Vanadates. Matter, **3**, 1614–1630.
43. Calvo, C. and Manolescu, D. (1973) Refinement of the structure of CuV_2O_6.

Acta Crystallogr. Sect. B Struct. Crystallogr. Cryst. Chem. **29**, 1743–1745.

44. McLaren, A.; Valdes-Solis T., Li G. & Tsang S. C. (2009) Shape and Size Effects of ZnO Nanocrystals on Photocatalytic Activity. *J. Am. Chem. Soc.* **131**, 12540–12541.